Solar Spectra Measurements and Surface Temperature Estimates

Syed Murtaza Husain
PHY 353L Modern Laboratory
Department of Physics
The University of Texas at Austin
Austin, TX 78712, USA

September 20, 2025

Abstract

Through the use of a low-resolution spectrometer, we measure solar spectral data and examine several features of the sun. We inspect the elemental absorption lines, in which we detect the presence of strong absorption lines for several elements, including Fe I, Mg I and H_β. Additionally, we use Wien's law to obtain an estimate of the temperature of the sun's surface temperature, for which we find an experimental value of $T = 5916 \pm 0.5\ K$, which is near the accepted value. We use calibrated spectral irradiance to obtain an estimate of Avogadro's number which disagrees with the accepted value, at $N_A = 1.62 \pm 0.002 \times 10^{25}\ mol^{-1}$. Finally, we examine the scattering effects of the atmosphere near sunset on the sun's spectra and find a significantly reduced blue/green band. From these measurements, we also calculate solar zenith angles and corresponding air mass values, extract wavelength-dependent optical depths, and determine scattering exponents $\alpha \approx 0.8$–1.1 ± 0.03, consistent with aerosol-dominated extinction in the lower atmosphere.

1 Introduction

1.1 Physics Motivation

The properties of the sun are of great importance, as they enable life on Earth and are responsible for delivering the energy that runs our biosphere. By studying the sun's attributes, we learn more about different scientific topics such as stellar and nuclear physics, astrochemistry, ecology, biology, and many others. Confirming well known properties of the sun improves our understanding of the natural world and validates procedures and reasoning that has been used for decades.

Historically, the study of the sun and the discovery of the solar spectrum has led to significant discoveries and involves many well-known names in physics. Isaac Newton, in the 17th century, showed that a glass prism can separate the components of sunlight and create the constituent colors of white light [8]. Following Newton's prism experiment, William Hyde Wollaston observed that the spectrum of sunlight through a prism contained dark lines [3].

These lines were cataloged by scientist Joseph von Fraunhofer, and physicists soon realized that these lines can be used to learn about the chemical composition of the incoming light [3]. This was the birth of spectroscopy as a science. Later, the solar constant, which was a measure of the sun's luminosity, was measured[19]. However, the initial attempts to measure the solar constant failed to account for absorption from the Earth's atmosphere, which led to a measurement of about half the currently accepted value [3].

The interaction of sunlight with Earth's atmosphere is equally important, as it governs how much solar energy reaches the ground and determines the color and brightness of the sky. The path length of sunlight through the atmosphere, known as the air mass, increases as the Sun approaches the horizon, and this longer path results in stronger attenuation of shorter wavelengths. These principles explain why the Sun appears white at noon, when

the air mass is small and attenuation is weak, but becomes red at sunset, when blue light is strongly scattered out of the direct path. By measuring optical depths and scattering exponents from our spectra, we connect our laboratory observations with the broader theory of atmospheric physics that has been developed for over a century.

Samuel Langley, in 1881, measured strong sunlight intensity variation with wavelength due to the absorption from Earth's atmosphere, and the effects of this were corrected for in future experiments [18]. Centuries of fascination with the properties of the sun have led to advances in the fields of optics, chemistry, astronomy, and has led to the birth of sciences such as spectroscopy. Because of the vital importance of these properties to our understanding of physics, we conduct our own measurements of the solar spectrum to both validate and better understand the associated physics.

1.2 Theoretical background

The most vital experimental tool to this procedure is a low-resolution spectrometer. A spectrometer is an instrument that can capture the elemental spectral lines of some object by utilizing light that interacts with the object [3]. Light that enters a spectrometer travels through an entrance slit and disperses through a diffraction grating, which separates the light by wavelength via path length difference. The separated light is focused onto a photo detector, which displays the intensity of each wavelength. This allows us to obtain characteristic absorption and emission lines that give us information about the elemental composition of the sample. The use of a low-resolution spectrometer allows us to obtain these characteristic absorption curves of light exiting the sun in a broad wavelength range that spans the entire visible spectrum. A high-resolution spectrometer is less desirable in this instance because the narrower wavelength range results in fewer observed absorption lines [3].

The photons that leave the sun and reach Earth are created within the core of the sun, and undergo tens of thousands of years of repeated random motion within the sun on average before leaving and streaming outward [1]. As the photons leave the sun, they interact with the sun's upper atmosphere, which will leave a mark in the form of an absorption spectrum on the photons when photons of certain wavelengths are absorbed by electrons in present molecules. This characteristic spectrum of sunlight 1 is made up of absorption lines known as Fraunhofer lines [7].

Wavelength (Å)	**Origin**
7594	terrestrial oxygen
6867	terrestrial oxygen
6563	hydrogen (Hα)
5896	neutral sodium (Na I)
5890	neutral sodium (Na I)
5270	neutral iron (Fe I)
4861	hydrogen (Hβ)
3968	ionized calcium (Ca II)
3934	ionized calcium (Ca II)

Table 1: A subset of the more easily indentifiable Fraunhofer lines, taken from [7]. These are made of strong absorption lines from elements in the sun's atmosphere.

Part of Planck's contribution toward the understanding of spectra was to quantify the spectral energy density at a given temperature with Planck's distribution law [5]:

$$u_v(\nu, T) = \frac{8\pi h\nu^3}{c^3} \frac{1}{e^{\frac{h\nu}{k_B T}} - 1}$$

Where $u_\nu(\nu, T)$ is the spectral energy density per unit frequency , ν is the frequency of radiation, T is the absolute temperature, h is Planck's constant, c is the speed of light in vacuum, and k_B is Boltzmann's constant. This can also be expressed for spectral radiance at an absolute temperature T for a given frequency ν [5]:

$$B_v(\nu, T) = \frac{2h\nu^2}{c^3} \frac{1}{e^{\frac{h\nu}{k_B T}} - 1}$$

Where k_B is the Boltzmann constant, h is the Planck constant, c is the speed of light and the units for spectral radiance are $W\ sr^{-1}\ m^{-2}\ Hz^{-1}$.

A blackbody emitter is an emitter of electromagnetic radiation, that emits varying amounts of energy across the EM spectrum. The sun is an example of a blackbody, although it has deviations from the idealized blackbody model[17]. The radiation emitted from the sun can thus be modeled as blackbody radiation, and we can obtain an estimate of the sun's temperature by examining the wavelength for which the sun's emitted radiation spectrum peaks and then applying Wien's law to this measure quantity.

Wien's law relates the peak wavelength emitted of a blackbody with the temperature, $\lambda_{max} T = 2.898 \times 10^{-3}\ m$. [17]

The Planck radiation of an object is the greatest amount of radiation that any blackbody emitter can emit from its surface at thermal equilibrium [5]. If this value is calculated theoretically, it can be compared to the actual radiance. The ratio of the two is known as the emissivity ϵ. In the case of the ideal black body, the emissivity would be 1 because it perfectly absorbs all incoming radiation. The sun can even be used to find a crude estimation for Avogadro's number. The approach for this is to obtain values for the photometric radiance, B, of the sun and the intensity, I, of the light, and solve for N_A in the following equation derived from Einstein's equation [15]:

$$B = I_0 \frac{2}{2\pi} \frac{M}{N_A} k^4 \frac{(n_0 - 1)^2}{\rho_0} z_0 \frac{1}{4\pi} \tag{1}$$

where I_0 is the solar intensity before atmospheric absorption, M is the molar mass of atmospheric gas, ρ_0 is gas density at altitude z_0, k is the wavenumber of the light, and n_0 is the refractive index of air. This relates the radiance of the sun against the absorption of atmospheric gases, and can be made to use the density to approximate the number of molecules in a mole, i.e Avogadro's number.

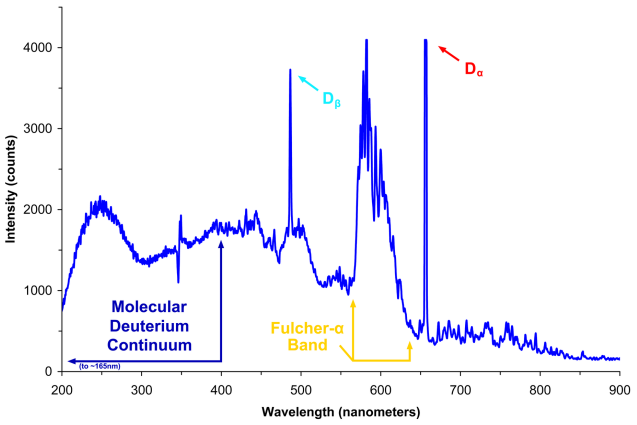

Figure 1: Example of spectrometer reading, spectrum of light emitted by a deuterium lamp, taken from [16]. Characteristic spectra can be seen in both emission and absorption lines.

Finally, understanding atmospheric effects on light is of vital importance. The Beer–Lambert law describes how the transmitted intensity decreases exponentially with the optical depth of the atmosphere. The optical depth is wavelength-dependent, with Rayleigh scattering from molecules scaling as λ^{-4} and aerosol scattering exhibiting a shallower dependence that can be parameterized by the Ångström exponent α. Large values of α correspond to fine particles and strong wavelength dependence, while smaller values indicate coarse aerosols and nearly gray extinction [6].

1.3 Our approach

Our approach is to utilize the low resolution HR2000 spectrometer[11], which has a response range of 200 to 1100 nm, to take spectrum readings of the sun. Before taking readings, we carry out an extensive calibration process in which we find calibration coefficients for the spectrometers and program them into the hardware. We must record the spectra, altitude of measurement, and ensure that we carry out the measurement on a day where weather conditions are amenable (low cloud cover).

We utilize data analysis techniques and the Oceanview software to examine the spectral peaks and features in the sun's spectrum and match them to the NIST database [9], by which we can make a rudimentary list of elements in the sun's atmosphere. In addition to this, we can take the highest peak of the spectrum and use Wien's law to get an estimate of the surface temperature of the sun. By using other theoretical estimates of the sun's intensity of light, we can also use equation 1 to estimate Avogadro's number. Additionally, we will test the spectrum at different times of day to observe atmospheric scattering effects, air mass estimates, and optical depths. As we complete our calibration process, we will also test properties of the spectrometer, such as how our calibration configurations change with the fiber optic cable connected, and the emission line locations vs nominal line locations from our HG-1 source lamp.

2 Experimental setup

2.1 Apparatus

Before we can begin taking measurements of the sun using our HR2000 spectrometer, we must calibrate the spectrometers using the Oceanview software[14] and the supplied HG-1 Argon-Mercury calibration lamp. A diagram of spectrometer internal components can be shown in figure 2. The experimental apparatus we create for this experiment involves using optical mounts to hold our fiber optic cable in place and allow us to stably measure incoming light. One innovation we introduce in our full

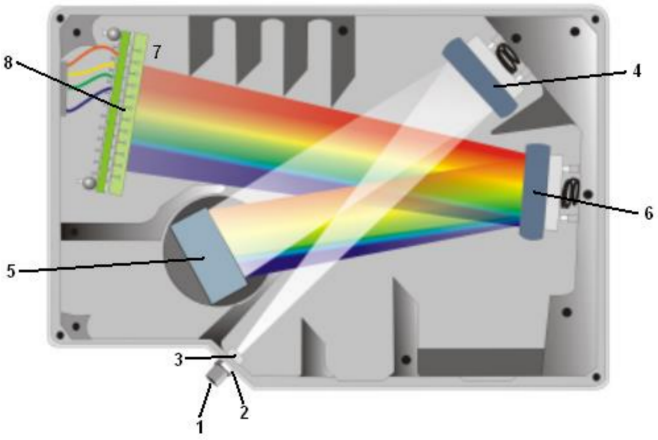

Figure 2: Diagram of HR4000, taken from [13], a high resolution spectrometer. Consists of of SMA connector **(1)**, slit **(2)**, filter **(3)**, collimating mirror **(4)**, grating **(5)**, focusing mirror **(6)**, L2 detector collection lens **(7)**, CCD detector **(8)**.

apparatus is including a polarizer on an optical mount, leveled to 0° using a bubble level also attached to the optical mount. By setting our fiber optic cable in a clamp that is facing directly upward perpendicular to the polarizer angle setting, we can freely vary the angle of the cable with respect to the angle of incidence of sunlight while also being able to measure the angular offset using the polarizer, allowing us to ensure we measure at 90° incidence. This setup is shown in figure 3.

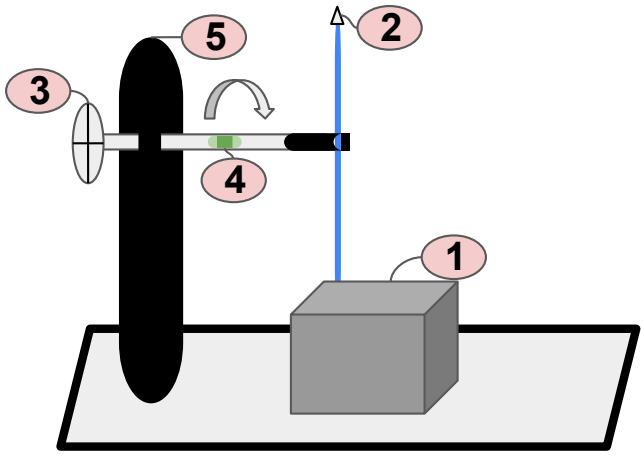

Figure 3: Diagram of apparatus. Consists of of HR2000 spectrometer **(1)**, fiber optic cable fastened upward **(2)**, polarizer for angle reading **(3)**, level to align polarizer **(4)**, optical stand with cylinder mount **(5)**.

2.2 Spectrometer Calibration

We utilize one of the lab computers to connect the HR2000 to the Oceanview software and view the dark spectra4a. We take two different dark spectra readings, one with the fiber optic cable connected, and one without. We note that there was a lack of equipment in the lab that might introduce error into the dark spectra, namely a missing fiber optic dark cap that is meant to help keep light from entering the spectrometer. Instead, we rely on cardboard beam blockers to accomplish this. These readings can be used to see the inherent error present in the device, and we can also determine by looking at the signal-to-noise ratio, how significant this is. We can see a significant peak in intensity at around 625 nm, suggesting that this device has some error, or the room light is being observed. We will address this in a data correction process post-observation.

To calibrate the device, we must create a fit for the following polynomial:

$$\lambda_p = I + C_1 p + C_2 p^2 + C_3 p^3 \tag{2}$$

where λ = the wavelength of pixel p, I = the wavelength of pixel 0, C_1, C_2, C_3 are the coefficients in (nm/pixel^n)[12]. This best fit must be programmed into the spectrometer before we take readings for the spectrometer to be fully calibrated. To calibrate, we will require a reference source that has known spectral lines and frequencies. The source we use for this is the HG-1 Argon-Mercury lamp that will shine a UV source into a fiber optic cable connected to the HR2000 [10]. We let the HG-1 remain on for 10 minutes as suggested by the user manual before connecting it via fiber optic cable to the HR2000. We then take a spectral reading from the source. We obtain peak readings from the Oceanview peak detector 2:

By using these peaks, we can calculate the calibration constants for the HR2000. By using the previously introduced polynomial λ_p 2, we use cubic regression to find the best fit parameters for our peak data points 5:

We can see that a very slight adjustment to the fit 5 is required to optimize the calibration of the spectrometer.

2.3 Spectrometer Error Correction

We can see that there is a significant spectrometer artifact present near 620 nm in the form of a large peak. This

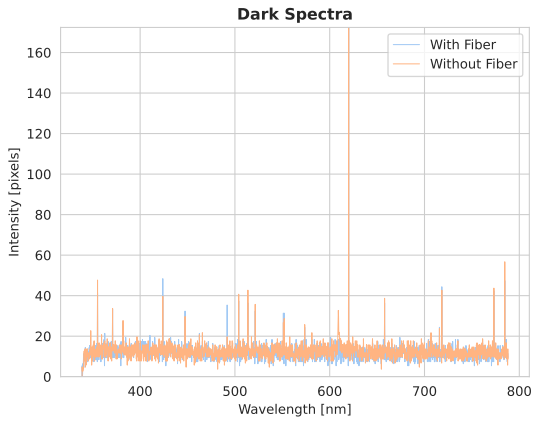

(a) Overlayed dark spectra for the HR2000, taken from Oceanview. An error peak can be seen at around 625 nm.

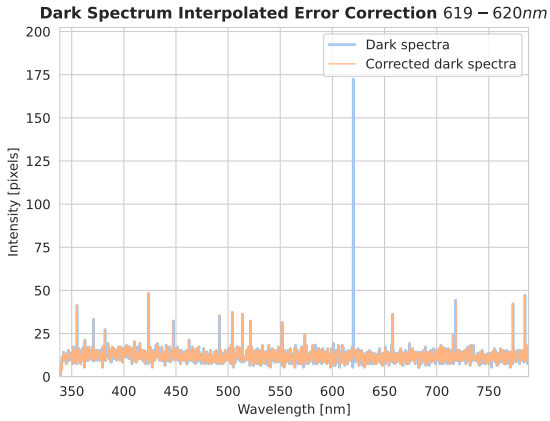

(b) Interpolation-corrected dark spectra with fiber optic cable connected, using interpolation between 619 $nm < \lambda < 620$ nm to remove error peak.

Figure 4: Dark spectra readings.

Peak Wavelength (nm)	Pixel Number
364.798	110
405.270	283
436.718	420
521.401	799
546.107	912
576.444	1052
625.130	1279
657.905	1433
694.583	1606
762.376	1926

Table 2: Calibration data: observed peak wavelengths and corresponding pixel numbers. Nominal line locations for the HR-1 lamp can be found in [10]. Error is ±0.05 nm.

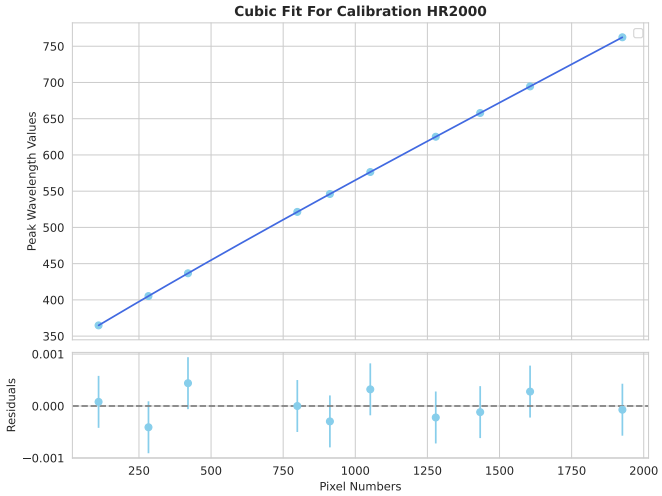

Figure 5: Parameter fit for HR2000 calibration. Fit parameters: $\lambda_p = (3.328 \times 10^{-9})x^3 - (1.685 \times 10^{-5})x^2 + (0.2402)x + 338.6$

error could become exponentially more pronounced when taking spectra of sources vs when taking a dark spectra. Given that it appears in our dark spectra, it is not an artifact of room lighting but is a fault within the hardware of our HR2000.

To account for this, we employ interpolation between 619 $nm < \lambda < 620$ nm to preserve the local data that could be important (such as the characteristic downward absorption slopes) while still removing the error significantly. Examples of this effect can be seen in 9a, and the interpolated fix for the peak can be seen in 9b. We also demonstrate the reduction in error by applying this correction method to our previously taken dark spectra readings 4b. Additionally, by matching the nominal emission lines to our data, we can determine a residual to find measurement error in the spectrometer 7. We find a max wavelength residual of ±0.49 nm, which can be considered our error moving forward.

2.4 Data Acquisition

Our data was collected using the high resolution HR2000 spectrometer from Ocean optics. To access the reading from this device, the use of the Oceanview software[14] is required, which we used a pre-installed version of present on a lab computer. We used a USB connector to interface the spectrometers with the lab computer and used a fiber optic cable to connect the HG-1 source[10] to either spectrometer.

To obtain all of our data in the spectra graphs, we utilized

the writeout feature of Oceanview to obtain text files that have information including the date and time of the measurement, boxcar width, integration time, trigger mode, etc. as well as the wavelength and pixel number in two different space separated columns.
The optical resolution of the HR2000 spectrometer is 0.035 nm as a nominal minimum error, and our integration time is set to 0.1 *sec* as is standard [11]. Given that the writeout feature of Oceanview often truncates precision, the 0.035 nm error will usually be superceded by the 0.05 nm least count of the measurements.

2.5 Data Collection

On two separate days, we take multiple spectra readings of the sun. The first day, we take readings at sunset, and the second day, we take readings at noon. We ensure that the weather conditions are appropriate to take readings of the sun, with low cloud cover and no precipitation. We also ensure that the fiber optic cable is held perpendicular to the sun's rays by using a polarizer and a bubble level as described in 3.

3 Data Analysis and Results

3.1 Sunlight Spectra Measurements and Temperature Estimate

During scheduled time at the PMA rooftop at noon, we obtained spectral measurements of the sun using our HR2000 6 and observed several dips in the sun's spectra that resemble characteristic absorption bands, as we expect. Additionally, we take a reading of the peak wavelength and find $\lambda_{peak} = 585.9 \pm 0.035\ nm$. From this, we use Wien's displacement law to estimate the sun's surface temperature to be $\lambda_{peak} = \frac{b}{T} \rightarrow T = 4946\ K$.

3.2 Spectra Line Classification

To classify the obtained emission dips from the solar spectrum, we use methodology from [2] to detect local dips that have a 20% or more dip and are separated by 10 nm. Detecting dips involves binning small wavelength ranges and finding any points that are significant deviations from averages of the intensity. Using a percentage dip allows us to fine-tune the strength of line we want to classify as significant absorption lines, and this process can be done to find weaker dips, but is then more prone to noise. This

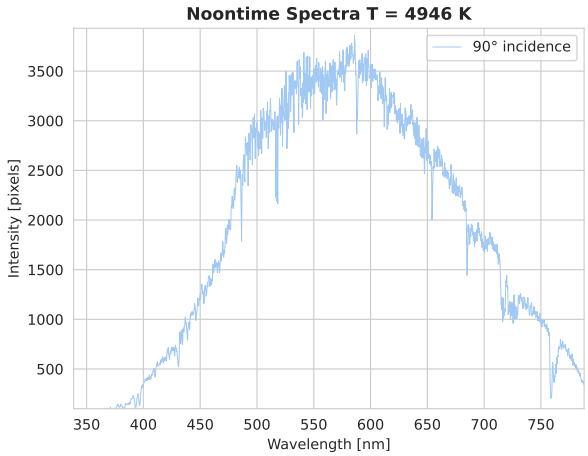

Figure 6: Interpolation-corrected noon spectra reading between 619 and 620 nm. Many absorption lines can be seen in the spectra all across the visible range

spectral line detection method yields 12 strong spectral absorption lines 7.

The table 3 shows the matches we obtained to NIST's spectra database. We note that the NIST database is saturated with many weawhk Fe I absorption lines, so there was significant filtering required based on line depth. This process to create an automated spectral line fitter querying NIST and detecting emission dips was a significant undertaking and the full plot with the matches and residuals to NIST is shown here 7.

3.3 Intensity Matching Using Calibration Files

To convert the counts from a spectrometer into spectral irradiance, we must follow one of the following the equations

$$\text{Nonlinear calibration: } B(\lambda) = C(\lambda)Cal(\lambda)\frac{I_\tau}{1000} \quad (3)$$

$$\text{Linear calibration: } B(\lambda) = (C(\lambda) + Cal(\lambda))\frac{I_\tau}{1000} \quad (4)$$

Where $C(\lambda), Cal(\lambda)$ are the counts and calibration parameter for intensity for a given wavelength.Usually, we would have a manufacturer specified intensity calibration file or would be able to create one by matching nominal intensity peaks to a lamp like the HG-1, but unfornately the HG-1 is only useful for wavelength calibration because there is no intensity table associated with it. However, the calibration parameters are given in a calibration file spe-

Measured Dip (nm)	Closest Line (nm)	Element	Residual (nm)
383.150	383.044580	Mg I	0.105420
392.958	393.170000	Na I	-0.212000
430.777	430.778900	Fe I	-0.001900
438.755	439.126200	Na I	-0.371200
486.452	486.273283	H I	0.178717
518.302	518.504780	Mg I	-0.202780
526.423	526.434530	Fe I	-0.011530
587.829	587.790640	Fe I	0.038360
654.041	654.029970	Fe I	0.011030
685.006	684.948400	Fe I	0.057600
716.341	715.867000	O I	0.474000

Table 3: Measured absorption dips compared with closest spectral lines. Residuals are calculated with respect to the closest match from the NIST spectra databse.

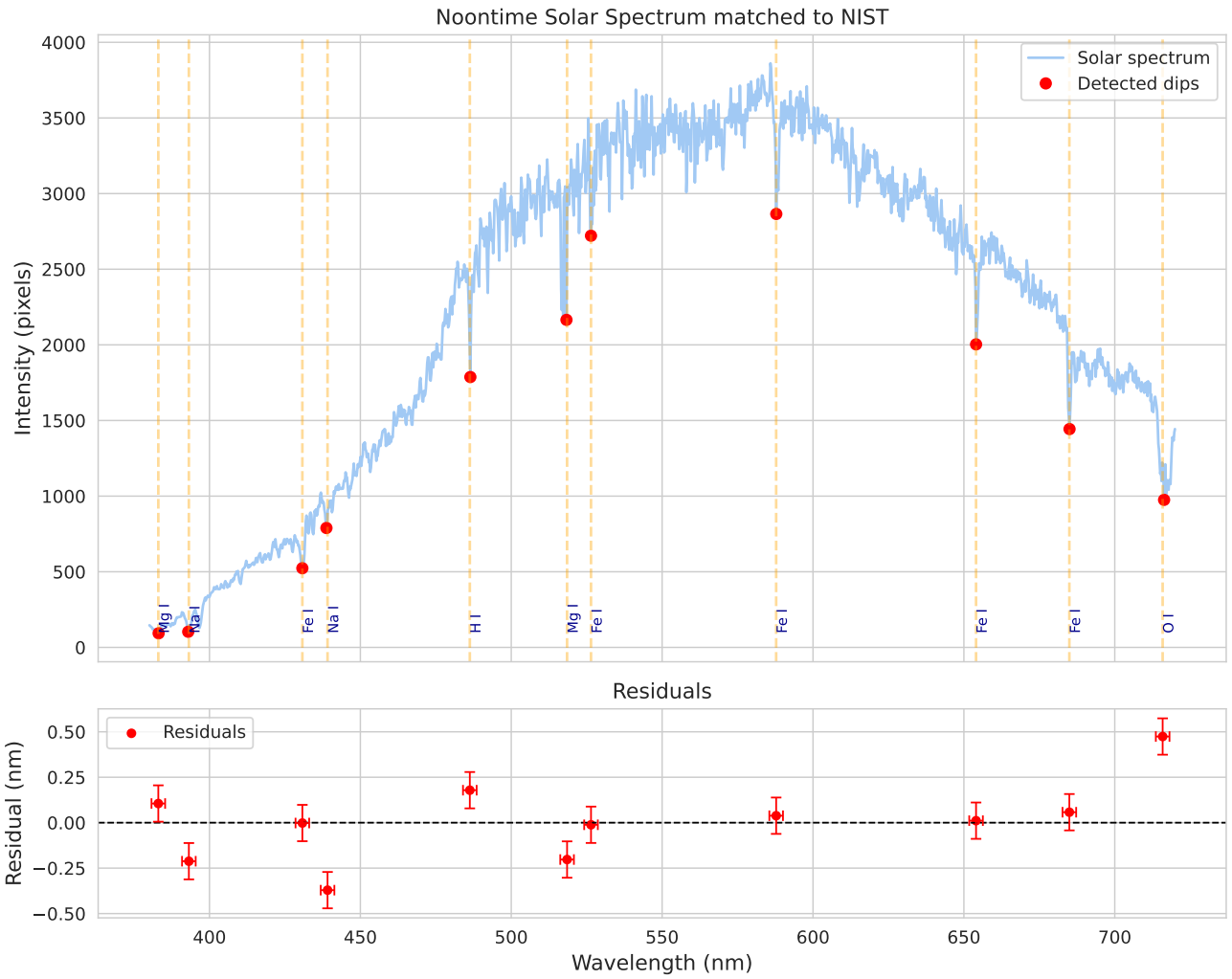

Figure 7: Noon spectra with dip classification and line matching to the NIST spectra database. Dips are classified with a 20% dip threshold and 10 nm minimum separation. Residuals are shown in the bottom plot.

cific to a manufactured spectrometer, and the provided data on the PHY353L course website are for a different Ocean optics spectrometer, the HR2B766. The provided file also appears to be a linear calibration file, with counts and wavelengths instead of correction factors. Then, we apply equation 4 and use the pixel values as $Cal(\lambda)$ regardless and note that this process might introduce significant error due to the spectrometer model mismatch. The results from this are shown in 8. Using this, we can find a new peak wavelength and calculate for the surface temperature using Wien's law once again. For this calculation, we find that $T = 5916\ K$ using our new peak.

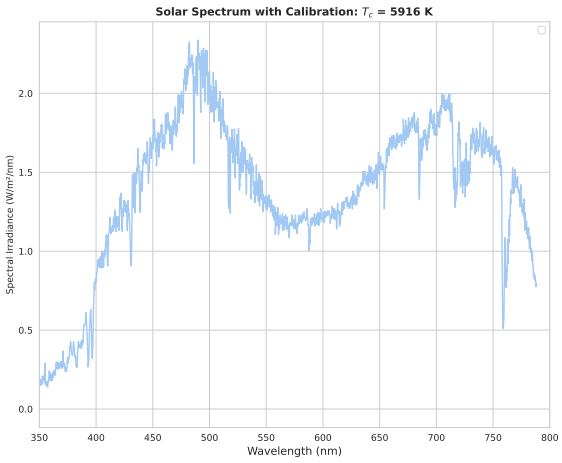

Figure 8: Sun spectra with intensity calibration The previously curved peak has broken into two peaks, with the lower wavelength peak being more prominent.

3.4 Calculating Avogadro's Number

Based on equation 1, we can calculate Avogadro's number using our absorption line data. Following the methodology of the original authors, who used the Mg I absorption lines to perform this, we choose the stronger Mg I absorption line at $\lambda = 518.3\ nm$ to calculate Avogadro's number. We also note that the 17th floor rooftop of the PMA is approximately 700 ft of elevation, which we use for our altitude parameter. The result we obtain is $N_A = 1.62 \pm 0.002 \times 10^{25}\ mol^{-1}$.

3.5 Sunset Spectra

Our initial attempt to obtain a spectrum using the HR2000 following successfully entering the calibration coefficients was unsuccessful due to the timing of our measurements. We took measurements at 7:00 PM, failing to account for the fact that the blue/green portion of the sun's spectrum would be diminished, as the atmosphere will preferentially scatter red light at this time of day. Nevertheless, we are able to obtain some spectra of sunset and apply our aforementioned error correction interpolation. The raw sunlight spectra are shown in figure 9a, and the interpolation processed curve for a 90° angle of incidence with sunlight is shown in figure 9b. Finally, we can see the difference between the sunset spectra and our noontime spectra. We note that there is a very large change in the overall intensity of the two readings, and can notice that proportionally to average intensity, the green/blue part of the spectrum is less intense during sunset due to scattering effects.

3.6 Atmospheric Properties

In addition to examining solar spectra, we also used our measurements to study several basic properties of Earth's atmosphere. First, using the geographic location of Austin, Texas (latitude 30.28°, longitude −97.74°, elevation 213 m), along with the times of our spectral measurements, we calculated solar zenith angles and corresponding air mass values. At noontime, we found air masses of $m \approx 1.17$–1.24, while at sunset the air masses increased to $m \approx 10.36$–10.71, reflecting the much longer atmospheric path length when the Sun is near the horizon.The results are showin in table 5.

Next, we used the Beer–Lambert law to derive the wavelength-dependent optical depth $\tau(\lambda)$ by comparing noon and sunset spectra. This will show us how strongly the atmosphere attenuates light at different wavelengths. Our results showed $\tau(\lambda)$ values in the range 0.2–0.3 across the visible spectrum, with larger values in the blue than in the red, consistent with scattering being stronger at shorter wavelengths. This is shown in figure 10b

Finally, we fit the wavelength dependence of $\tau(\lambda)$ to the Ångström power law, $\tau(\lambda) = \beta\lambda^{-\alpha}$, to obtain the scattering exponent α. The results are showin in table 4. We found values in the range $\alpha \approx 0.8$–1.1, depending on the sunset spectrum and whether calibration was applied. These values are typical of aerosol-dominated

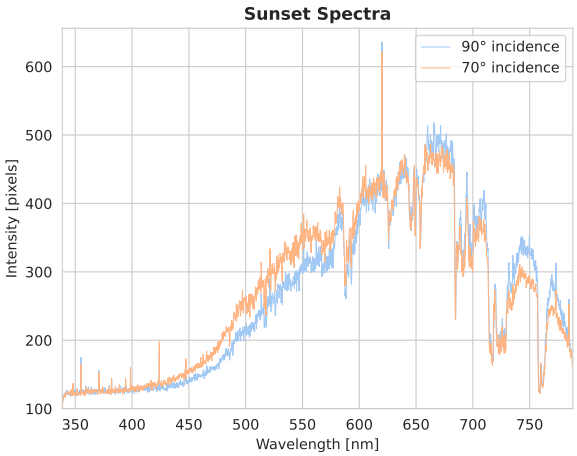

(a) Sunset spectrum with 620 nm artifacts.

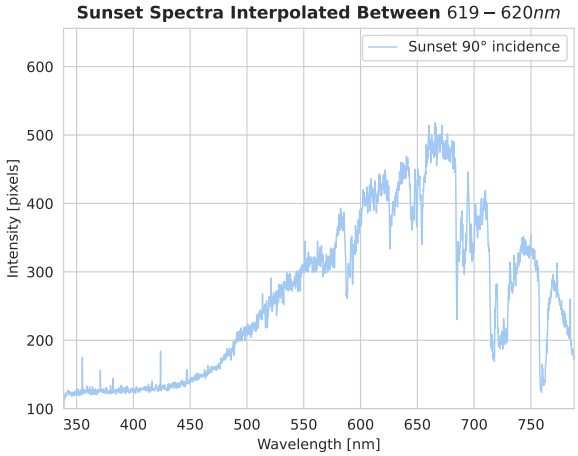

(b) Sunset spectrum with interpolated error correction.

Figure 9: Comparison of HR2000 sunset spectra before and after correction. The error peak at 620 nm is removed in the corrected spectra.

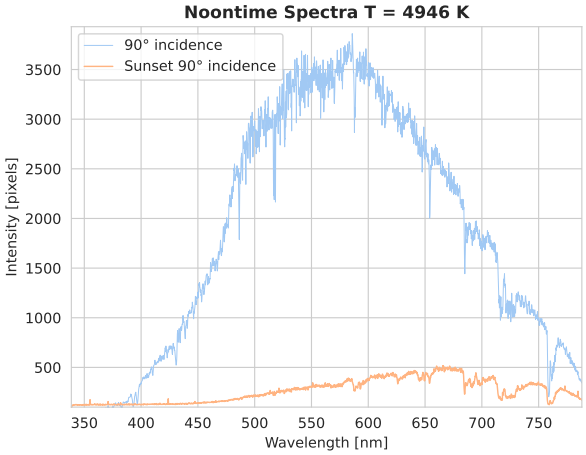

(a) Sunset spectrum vs noontime spectrum. The sunset spectrum has a significantly reduced blue/green band due to atmospheric scattering effects, as well as a much lower overall intensity.

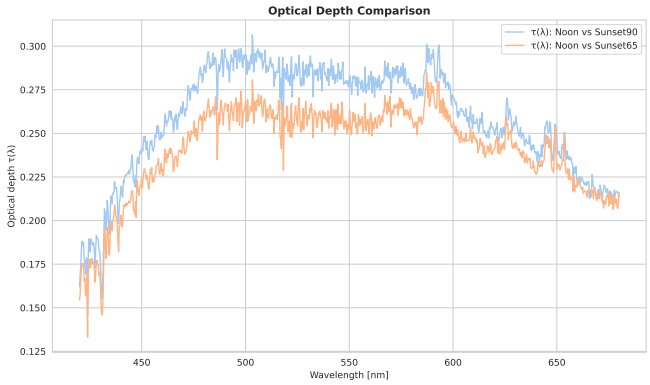

(b) Optical depth as a function of wavelength given by the Beer Lambert law. Results imply that scattering is stronger at blue wavelengths.

extinction in the lower atmosphere, which is much flatter than the pure Rayleigh scattering dependence ($\alpha \approx 4$). The results are consistent with the visual observation of diminished blue/green light during sunset, as aerosols and longer air mass paths preferentially remove shorter wavelengths from the direct solar beam path.

Calibration	**Sunset**	$\boldsymbol{\alpha}$ (420–680 nm)	$\boldsymbol{\alpha}$ (450–600 nm)
No	90°	0.26	0.77
No	65°	0.67	1.04
Yes	90°	0.47	0.82
Yes	65°	0.88	1.09

Table 4: Ångström scattering exponents α derived from optical depth fits. Values near 1 are consistent with aerosol extinction, and higher values would be expected for fine particles and lower values for coarse-mode scattering.

Spectrum	Air Mass Value
Noon 90°	1.240
Noon 65°	1.170
Sunset 90°	10.363
Sunset 65°	10.712

Table 5: Calculated air mass values for noontime and sunset observations. The large increase in air mass between noon and sunset reflects the longer atmospheric path length at low solar elevation.

4 Summary and conclusions

4.1 Spectra Comparison to Known Lines

Our spectra of the sun shows remarkable similarity in strong absorption lines to those in [7] as expected, with low residuals within $\pm 2.3\ nm$. The matched lines using the NIST database correspond to the correct lines barring 3 exceptions that detect a false Na I, Mg I, and O I line. The latter can be explained by being very near the wavelength detection limit of the spectrometer and giving an unreliable reading, while the first two are likely an artifact of the NIST database filtering of weak Fe I lines being at slightly different thresholds than the listed lines and being filtered out during the query. The residuals are shown in figure 11.

4.2 Results and Brief Discussion

The estimate we obtained for the surface temperature of the sun, $5916 \pm 0.5\ K$, is very close to the accepted known temperature of $5772\ K$. The error can be explained due to atmospheric absorption effects, and in our follow-up intensity matching procedure, we corrected for this by tuning our $Cal(\lambda)$ to corrected data. For our estimate of Avogadro's number, we were able to use our calibrated spectral irradiance values and absorption line detections to obtain an estimate of Avogadro's number, with a value of $N_A = 1.62 \times 10^{25}\ mol^{-1}$. This is a significant disagreement with the accepted value, but is close to the order of magnitude, and we note that small changes in measured spectra line placements and chosen spectra lines can introduce a large difference in results due to the k^4 dependence in 1. Disagreements with the accepted value of $N_A = 6.02 \times 10^{23}$ could be due to experimental error, unfavorable atmospheric conditions, and lack of a precise altitude measurement. For our study of atmospheric properties, we first calculated the air mass values from the solar zenith angle at our measurement times. We obtained values of $m \approx 1.17$–1.24 for noontime spectra and $m \approx 10.36$–10.71 for sunset, consistent with the expected increase in path length as the Sun approaches the horizon. From these spectra we then derived the wavelength-dependent optical depth, finding values of $\tau(\lambda)$ in the range of 0.2–0.3 across the visible spectrum, with stronger attenuation at shorter wavelengths. These values are consistent with known optical depths for the atmosphere at low altitude and moderate aerosol loading. Finally, we fit the Ångström power law to the derived optical depths to obtain the scattering exponent α. We found values of $\alpha \approx 0.8$–1.1, which indicates aerosol-dominated extinction in the lower atmosphere. This is in agreement with the observed reduction of the blue/green band in the sunset spectra and supports the interpretation that aerosols, rather than pure Rayleigh scattering, control the optical properties of the sky near the horizon.

4.3 Intensity Matching Using ASTM G173-03

Because the calibration parameters for our spectrometer were unobtainable and we had to rely on those for a different model, we can attempt to create our own nonlinear $Cal(\lambda)$ using known spectra of the sun. Using the ASTM G173-03 ground spectrum [4] of the sun, we introduce a bin-normalization protocol that will take averages of the reference spectrum to create a calibration file. The reference spectrum, our previous 12 was used additively in our data analysis, while this reference is a nonlinear correction. Using this, we can find a new peak wavelength and calculate for the surface temperature using Wien's law once again. We find that $T = 6009\ K$ using our peak, as opposed to the ASTM G173-03 peak, which found $T = 5845\ K$. Notably, using this correction actually pushes our T estimate farther from the accepted value.

4.4 Conclusion

The goals of this experiment were to determine the chemical composition of the sun's surface using its spectral features, estimate the surface temperature of the sun using our peak recorded wavelength and Wien's law, and estimate Avogadro's number using spectral irradiance, all through the use of a low-resolution spectrome-

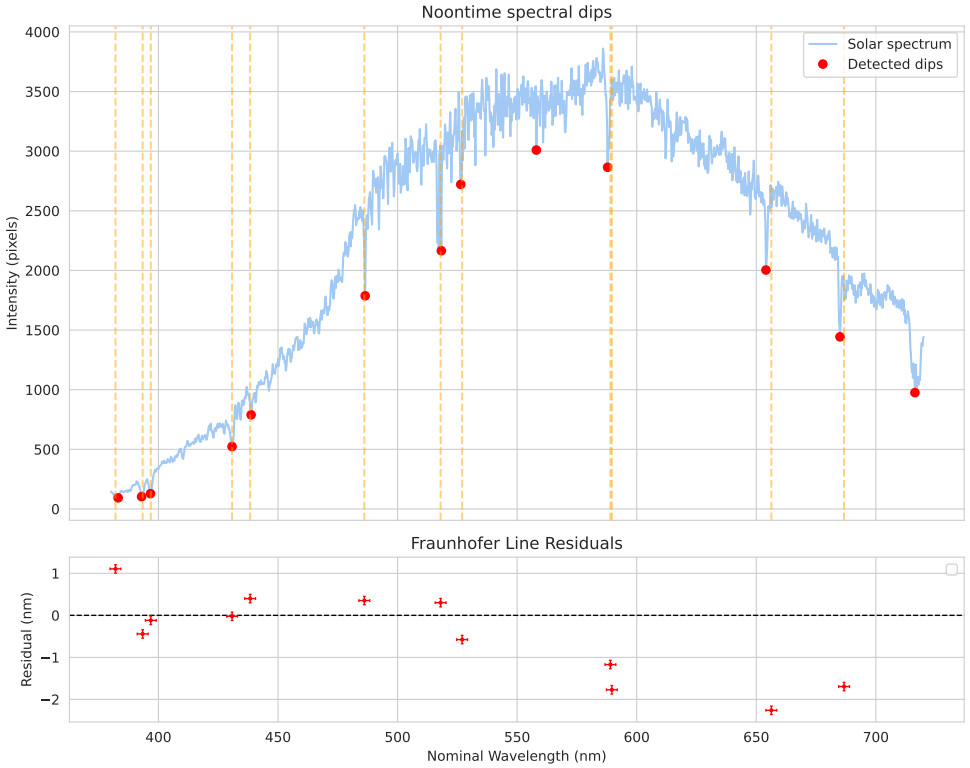

Figure 11: Residuals for detected lines vs Fraunhofer lines using nominal wavelengths from [7]. Residuals are within $\pm 2.3\ nm$, showing very good agreement.

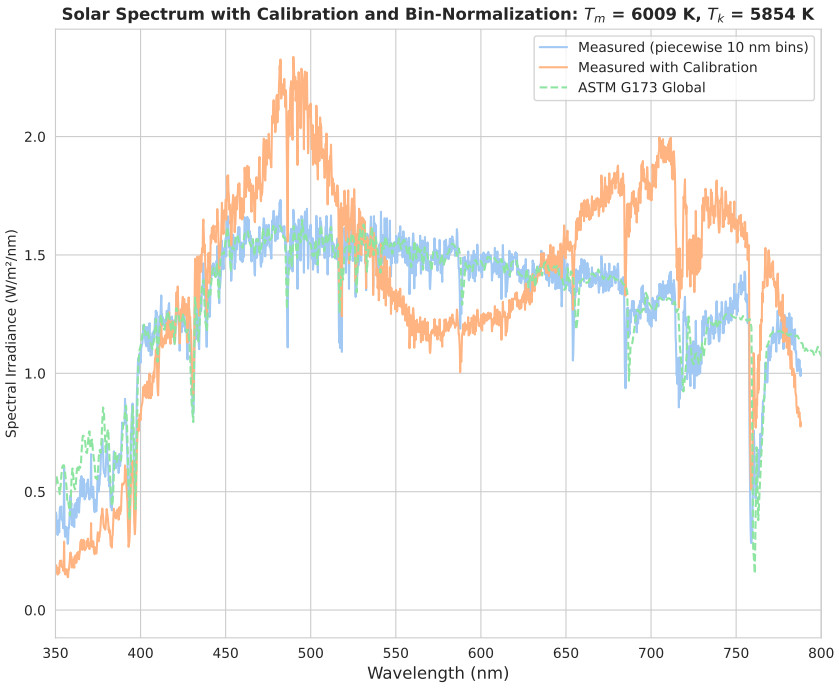

Figure 12: Sun spectra with ASTM reference, bin-normalization, and file calibration. The ASTM and normalized spectra have a much more flat distribution vs the calibrated spectra's dual peaks.

ter. To accomplish this, we performed spectrometer calibration, accounted for time of day and weather conditions, and created a lengthy data analysis pipeline. Our results of $T = 5916 \pm 0.5\ K$ for surface temperature aligns closely with the accepted value, while our value of $N_A = 1.62 \times 10^{25}\ mol^{-1}$ disagrees with the accepted value but is close to an order of magnitude estimate. Throughout the data collection process, we also obtain some insight into scattering effects and angle of incidence variations with data collection. These results demonstrate the ubiquity and importance of studying the sun's properties, and has been a valuable exercise in data collection and independent laboratory procedure.

4.5 Future Work Considerations

Future work might consider using recommended manufacturer calibration for spectrometer $Cal(\lambda)$ mappings to avoid having to use suboptimal to compute the spectral irradiance being measured by their spectrometer, precisely measuring their altitude when estimating Avogadro's number, obtaining an optical fiber cap to take dark spectra readings, and correcting for the atmosphere's effects. Another potential improvement is using a wider array of spectrometers, both lower resolution instruments that can detect infrared and ultraviolet spectra as well as higher resolution ones that can focus on narrow bands to view specific absorption lines in more detail.

Acknowledgements: Thanks to my partner, Adin Viera, and to our lab TAs, Joshua and Oorie.

References

[1] John A. Duffie and William A. Beckman. *Solar Engineering of Thermal Processes*. 4th ed. Hoboken, NJ: Wiley, 2013.

[2] E. A. Gurtovenko and R. I. Kostik. "Formation depths of Fraunhofer lines". In: *arXiv preprint arXiv:1505.00975* (2015). URL: https://arxiv.org/abs/1505.00975.

[3] G. R. Harrison. *Spectroscopy*. Cambridge, MA: MIT Press, 2000.

[4] ASTM International. "Standard Tables for Reference Solar Spectral Irradiances: Direct Normal and Hemispherical on 37° Tilted Surface". In: (). URL: https://store.astm.org/g0173-03r20.html.

[5] Friedrich Lenz. *Statistical Physics of Particles*. Princeton, NJ: Princeton University Press, 2013.

[6] K. N. Liou. *An Introduction to Atmospheric Radiation*. 2nd ed. San Diego, CA: Academic Press, 2002.

[7] Charlotte E. Moore. *The Solar Spectrum*. Washington, DC: National Bureau of Standards, 1945.

[8] Isaac Newton. *Opticks*. London: Sam. Smith and Benj. Walford, 1704.

[9] NIST. *Atomic Spectra Database*. URL: https://www.nist.gov/pml/atomic-spectra-database.

[10] Ocean Optics. *HR-1 Datasheet*. URL: https://www.artisantg.com/info/Ocean_Optics_HG_1_Datasheet_20225248238.pdf.

[11] Ocean Optics. *HR2000 Data Sheet*. URL: https://www.oceanoptics.jp/technical/oem_datasheet_HR2000+.pdf.

[12] Ocean Optics. *HR2000 Installation and Operation Manual*. 2024. URL: https://www.oceanoptics.com/wp-content/uploads/2024/12/HR2000Plus.pdf.

[13] Ocean Optics. *HR4000 Operation Manual*. 2024. URL: https://www.oceanoptics.com/wp-content/uploads/2024/12/HR4000.pdf.

[14] Ocean Optics. *OceanView Software Quickstart Guide*. URL: https://photos.labwrench.com/equipmentManuals/14863-5822.pdf.

[15] Marco A. C. Potenza. "The daylight sky and Avogadro's number". In: *European Journal of Physics* 36.6 (2015), p. 065040. DOI: 10.1088/0143-0807/36/6/065040. URL: https://air.unimi.it/bitstream/2434/339120/2/MPotenza_EuropeJournPhysics_DaylightSkyAvogadro_2015.pdf.

[16] researchgate. "Deuterium Lamp Spectrum". In: (). URL: https://www.researchgate.net/figure/The-spectrum-of-the-deuterium-lamp-In-this-diagram-the-position-of-the-wavelengths-is_fig4_355405323.

[17] George B. Rybicki and Alan P. Lightman. *Radiative Processes in Astrophysics*. New York: Wiley-VCH, 1979.

[18] Michael Stix. *The Sun: An Introduction*. 2nd ed. Berlin, Germany: Springer, 2002.

[19] Harold Zirin. *Astrophysics of the Sun*. Cambridge, UK: Cambridge University Press, 1992.